PLOS | ONE

RESEARCH ARTICLE

Dependence of DCE-MRI biomarker values on analysis algorithm

Chaan S. Ng[1]*, Wei Wei[2], James A. Bankson[3], Murali K. Ravoori[1], Lin Han[1], David W. Brammer[4], Sherry Klumpp[4], John C. Waterton[5¤], Edward F. Jackson[6]

1 Department of Radiology, University of Texas M.D. Anderson Cancer Center, Houston, Texas, United States of America, **2** Department of Biostatistics, University of Texas M.D. Anderson Cancer Center, Houston, Texas, United States of America, **3** Department of Biostatistics Imaging Physics, University of Texas M.D. Anderson Cancer Center, Houston, Texas, United States of America, **4** Department of Biostatistics Veterinary Medicine and Surgery, University of Texas M.D. Anderson Cancer Center, Houston, Texas, United States of America, **5** Personalised Healthcare and Biomarkers, AstraZeneca, Alderley Park, Cheshire, United Kingdom, **6** Department of Medical Physics, University of Wisconsin, Madison, WI, United States of America

¤ Current address: Biomedical Imaging Institute, University of Manchester, Manchester Academic Health Sciences Centre, Manchester, United Kingdom
* cng@mdanderson.org

OPEN ACCESS

Citation: Ng CS, Wei W, Bankson JA, Ravoori MK, Han L, Brammer DW, et al. (2015) Dependence of DCE-MRI biomarker values on analysis algorithm. PLoS ONE 10(7): e0130168. doi:10.1371/journal.pone.0130168

Editor: Zhuoli Zhang, Northwestern University Feinberg School of Medicine, UNITED STATES

Received: January 14, 2015

Accepted: May 18, 2015

Published: July 24, 2015

Data Availability Statement: All relevant data are available from the Harvard Dataverse (http://dx.doi.org/10.7910/DVN/PPIACV).

Funding: This work was supported by MDACC - AstraZeneca Research Collaboration Alliance; Cancer Center Support Grant (P30-CA016672); John S. Dunn Sr. Distinguished Chair in Diagnostic Imaging. AstraZeneca provided support in the form of salary for author JCW.

Competing Interests: CS Ng and EF Jackson received research funding from AstraZeneca. CS Ng receives research funding from GE Healthcare. JC

Abstract

Background

Dynamic contrast-enhanced MRI (DCE-MRI) biomarkers have proven utility in tumors in evaluating microvascular perfusion and permeability, but it is unclear whether measurements made in different centers are comparable due to methodological differences.

Purpose

To evaluate how commonly utilized analytical methods for DCE-MRI biomarkers affect both the absolute parameter values and repeatability.

Materials and Methods

DCE-MRI was performed on three consecutive days in twelve rats bearing C6 xenografts. Endothelial transfer constant (K^{trans}), extracellular extravascular space volume fraction (v_e), and contrast agent reflux rate constant (k_{ep}) measures were computed using: 2-parameter ("Tofts" or "standard Kety") *vs*. 3-parameter ("General Kinetic" or "extended Kety") compartmental models (including blood plasma volume fraction (v_p) with 3-parameter models); individual- *vs*. population-based vascular input functions (VIFs); and pixel-by-pixel *vs*. whole tumor-ROI. Variability was evaluated by within-subject coefficient of variation (wCV) and variance components analyses.

Results

DCE-MRI absolute parameter values and wCVs varied widely by analytical method. Absolute parameter values ranged, as follows, median K^{trans}, 0.09–0.18 min^{-1}; k_{ep}, 0.51–0.92 min^{-1}; v_e, 0.17–0.23; and v_p, 0.02–0.04. wCVs also varied widely by analytical method, as follows:

Waterton was employed by AstraZeneca. This does not alter the authors' adherence to PLOS ONE policies on sharing data and materials.

mean K^{trans}, 32.9–61.9%; k_{ep}, 11.6–41.9%; v_e, 16.1–54.9%; and v_p, 53.9–77.2%. K^{trans} and k_{ep} values were lower with 3- than 2-parameter modeling (p<0.0001); k_{ep} and v_p were lower with pixel- than whole-ROI analyses (p<0.0006). wCVs were significantly smaller for v_e, and larger for k_{ep}, with individual- than population-based VIFs.

Conclusions

DCE-MRI parameter values and repeatability can vary widely by analytical methodology. Absolute values of DCE-MRI biomarkers are unlikely to be comparable between different studies unless analyses are carefully standardized.

Introduction

Imaging biomarkers can assess tumor perfusion and permeability, and are useful in assessing response to therapy [1]. In particular, dynamic contrast-enhanced magnetic resonance imaging (DCE-MRI) provides biomarkers of tissue perfusion with proven utility in oncologic imaging, including the assessment of treatment responses and development of anti-cancer therapies [2–4]. However, these biomarkers are little-used outside the single-center setting, probably because different implementations of the imaging acquisition and analysis have not been shown to provide comparable biomarker values.

The DCE-MRI technique has been, and can be, used in clinical and pre-clinical settings, the latter in particular where novel therapeutic agents are under investigation [5–9]. In both settings, quantitative evaluations of the changes in derived tissue perfusion biomarkers have often been the main objectives. While any one study will use the same algorithm and analytical implementation for all subjects pre- and post-therapy, there is little consistency between studies. Although biomarker values are quoted in absolute units (e.g. k^{trans} /min^{-1}), it is unclear to what extent absolute values reported from different studies are comparable. In this study we evaluated three important analysis options: the choice of model, the method of derivation of the input function, and the algorithm for aggregating pixel-wise data to derive whole-tumor biomarkers.

The technique of DCE-MRI depends on acquiring dynamic MRI data and applying an appropriate physiological model to that data. A variety of tracer kinetic models have been developed for these purposes; two commonly utilized models are variably termed the Tofts and Kermode, "standard" Kety, or 2-parameter model [10–12], and the generalized kinetic, "extended" Kety, or 3-parameter model [13]. Application of these models allows derivation of specific MRI perfusion parameters, such as the endothelial transfer constant (K^{trans}), the contrast agent reflux rate constant (k_{ep}), the extracellular extravascular space volume fraction (v_e), and the blood plasma volume fraction (v_p).

Model-based derivations of DCE-MRI parameters require a vascular input function (VIF). Obtaining reliable VIF data has been, and is, challenging, particularly in pre-clinical settings where even the central vessels, *e.g.*, aorta and inferior vena cava, are extremely small. Imaging artifacts and the high cardiac rate of small animals add to the challenges. The unreliable nature of some VIFs from individual subjects can potentially confound the overall estimates of perfusion parameter values. In these situations, model or population-based VIFs have been suggested [10,14–20].

Tissue perfusion parameters for a region of interest (ROI) can be derived on a "whole tumor" or "pixel-by-pixel" basis. Pixel-level data in principle offers a more detailed evaluation

and allows for intratumoral assessment of the heterogeneity of each measured parameter [20]. It is, however, prone to the potential challenges of additional computation time and signal-to-noise ratio limitations.

In this study, we computed DCE-MRI parameter values utilizing all combinations of the above methods on DCE-MRI images obtained on three successive days in each of twelve rat xenografts. Absolute parameter values and repeatability were compared. An understanding of repeatability provides data for assessing study results and for study design (namely, determining sample sizes).

Our objectives were to compare the absolute values and test-retest repeatability of DCE-MRI parameters analyzed by two tracer kinetic models (2-parameter *vs*. 3-parameter), two different VIF input strategies (individual- vs. population-based), and two tissue ROI approaches (whole tumor *vs*. pixel-by-pixel) in a rat tumor model.

Materials and Methods

The study was approved by the Institutional Animal Care and Use Committee (IACUC) of The University of Texas M.D. Anderson Cancer Center (Protocol Number 09-06-12041). C6 rat glioma cells were obtained from the American Type Culture Collection (Manassas, VA, USA). Five thousand C6 cells were injected subcutaneously into male Crl: NIH-*Foxn1*^{rnu} T-cell deficient, athymic nude rats (Charles River, Wilmington, MA). Rats weighted approximately 220 grams at the time of the experiment. Cells were injected in the flank region, at the approximate axial level of the inferior aspect of the kidneys and distal aorta. Tumor measurements were undertaken using calipers, and tumors allowed to grow until they reached a nominal size of approximately 1 cm diameter. Each rat then underwent DCE-MRI on three consecutive days. Animals were scanned in batches of 5 to 6 animals per cohort.

Animals were placed in an MRI-compatible cradle in which a 5-cm hole had been cut into which the subcutaneous tumor could be located. Hair from around the tumor was shaved, and the region of the tumor was placed in a "bath" of ultrasound gel to minimize air/tumor susceptibility effects in the MRI imaging studies. A temperature controlled pad was placed underneath the animals, and the animals were gently immobilized with tape. Animals were anesthetized with 1–2% isoflurane in a 1 l/min O_2 flow, and imaging was undertaken in free respiration throughout. The imaging volume was targeted on the central portion of the tumor.

An estimate of tumor volume (cm^3) was obtained from the formula for a spheroid, *i.e*., $(\pi^*X^*Y^2)/6000$, where X and Y (in mm) were orthogonal tumor diameter measurements.

Data from a total of 12 sets of three consecutive days of scanning were obtained: 10 rats underwent three consecutive DCE-MRI studies during a single week period; one animal underwent the three consecutive DCE-MRI studies in two separate weeks. There was a technical scanning failure on one MRI scan visit in one rat. The median size of tumors was 0.67 cm^3 (range 0.09–1.53 cm^3). At the end of the study, the rats were euthanized humanely by inhalation of carbon dioxide.

DCE-MRI technique

MRI studies were undertaken using a 7.0 Tesla / 30 cm bore dedicated animal MRI scanner (Bruker BioSpin, Billerica, MA). The MR scanning protocol consisted of the acquisition of sagittal and axial T_2-weighted images, axial T_1-weighted images, axial DCE-MRI images, and post-Gd axial T_1-weighted images. For the DCE-MRI acquisition, a 3D fast spoiled gradient echo sequence was used with TE = 1.7ms, TR = 10ms, 15° excitation pulse, 16-mm slab thickness (yielding eight 2-mm slices), 128 x 80 matrix, and 60mm x 50mm field of view. To reduce artifacts in the VIF from inflow effects, a spoiled hermite magnetization preparation pulse was

applied to excite an 8-cm slab located 2 mm caudal to the DCE-MRI slice package [21]. The temporal resolution was 6.4s, with total scan time of 320s (50 x 6.4s). Contrast agent was administered after 10 baseline scans were acquired.

The MRI contrast agent was delivered through a tail vein as follows: 0.2 mmol/kg dose of gadopentetate dimeglumine (Magnevist, Bayer Healthcare Pharmaceuticals, Wayne, NJ), via an MR-compatible injection system (Harvard Apparatus, PHD 2000 Programmable, Plymouth Meeting, PA). For a 200-gram rat, for example, 200 μl of contrast media at 1:5 dilution of Magnevist:saline was administered over a period of 10 seconds. This was followed by a saline flush of the same volume and injection rate.

The acquired DCE-MRI data were analyzed using the Kinmod module (version 3.0) within the CineTool (version 8.2.1) environment (GE Healthcare, Waukesha, WI), utilizing two tracer kinetic models (2-parameter *vs*. 3-parameter), two VIF input strategies (population-based *vs*. individual-based), and two ROI approaches (whole tumor cross-sectional ROI *vs*. pixel-by-pixel within the ROI).

Tracer kinetic models: two- vs. three- parameter

Analyses were undertaken using two standard two-compartment tracer kinetic models: a) 2-parameter ("Tofts" or "standard Kety") and b) 3-parameter ("General Kinetic" or "extended Kety") model.

a) 2-parameter model:.

$$C_t(t) = K^{trans} \int_0^t C_p(t') e^{-\left[\frac{K^{trans}(t-t')}{v_e}\right]}\, dt'$$

where $C_t(t)$ is the tracer concentration in tissue, $C_p(t)$ is the tracer concentration in arterial blood plasma, K^{trans} is the volume endothelial transfer constant between blood plasma and extravascular extracellular space (in min^{-1}), and v_e is the extravascular extracellular tissue volume fraction (dimensionless).

This model is variably named the Tofts and Kermode, Larsson, or "standard (flow-limited)" Kety model [10–12].

b) 3-parameter model:.

$$C_t(t) = v_p C_p(t) + K^{trans} \int_0^t C_p(t') e^{-\left[\frac{K^{trans}(t-t')}{v_e}\right]}\, dt'$$

where the additional term, v_p, is the blood plasma volume fraction (dimensionless).

This model is otherwise named the General Kinetic Model (GKM), or "extended" Kety model [12].

For both models, the contrast agent reflux rate constant, k_{ep} (in min^{-1}) = K^{trans} / v_e.

Vascular input function: individual vs. population

We evaluated two commonly utilized vascular input functions (VIF): a) individually measured, and b) population-based.

a) Individually measured VIF. For each animal and time point, the VIF was obtained using a mask ROI defined by the study radiologist (CSN, more than 15 years' experience) containing the inferior vena cava in an imaging section near the center of the DCE-MRI scan volume. From the mask ROI, the VIF was determined using an automated VIF identification algorithm within the Kinmod module (Figs 1A and 2A). The VIF represents vascular gadopentetate concentration measured in units of signal intensity change from baseline as a function of time, *i.e.*, $\Delta SI(t) = SI(t) - SI(baseline)$, where $SI(baseline)$ was obtained by averaging the signal

Figure 1a

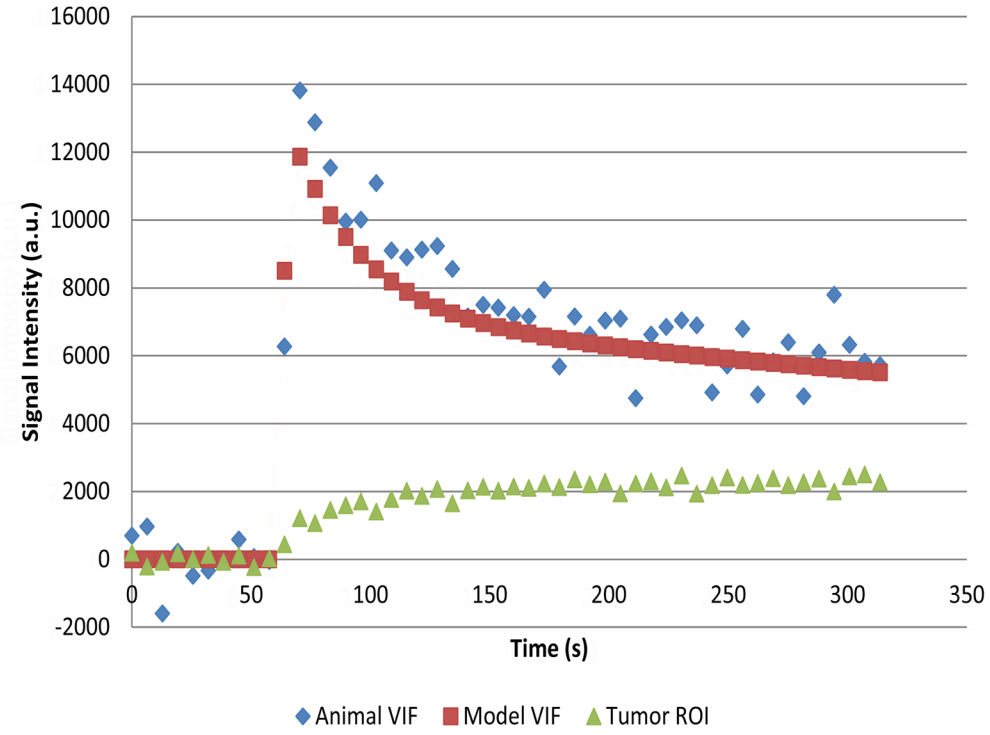

Figure 1b

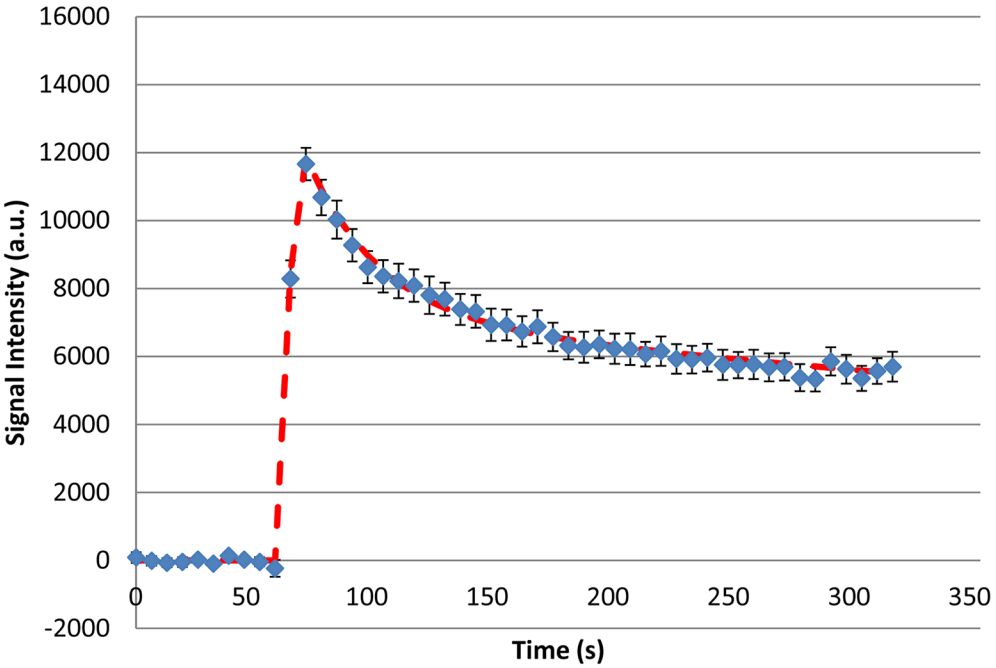

Fig 1. Example of signal intensity profiles. A) Vascular input function (VIF) from a representative individual animal (blue), and population average (red). Green symbols: tumor whole ROI data. Y-axis in units of signal intensity change from baseline, *ΔSI*. B) Average signal intensity change (VIF) from all animals and scan

visits, including the standard error, for each data point (blue); and the fitted population-average VIF curve (red line). Y-axis in units of signal intensity change from baseline, *ΔSI*.

doi:10.1371/journal.pone.0130168.g001

intensity from frames 5–10, after achieving steady state but prior to contrast agent administration [22].

b) Population average VIF. The population-based VIF was derived from the individual VIFs (discussed above) obtained from all 12 rats of the study cohort and all available scan visits, *i.e.*, 3 visits per rat. The individual VIF curves for all animals were averaged and the resulting data fitted to a biexponential function resulting in a population VIF given by

$$C_p(t) = 0.64\, e^{-0.0333t} + 0.42\, e^{-0.0010t}$$

where t is in seconds and $C_p(t)$ is in units of signal intensity change, $\Delta SI(t)$ (Fig 1B). The short and long component amplitude and clearance rates thus determined were in good agreement with previously published data [23,24].

Tumor ROI approaches: pixel-by-pixel vs. whole

ROIs were drawn by a single observer (CSN) using an electronic cursor and mouse for the three central slices of tumor for each rat. DCE-MRI parameters were computed using all combinations of the two tracer kinetic models and the two VIF methods above, using the same set of ROIs for each tumor. DCE-MRI parameter values were obtained for each tumor ROI based on: a) whole cross section ROI data, and b) pixel-by-pixel data within the ROI. In both cases, the values of $C_t(t)$ represent the tissue gadopentetate concentration measured in units of signal intensity change from baseline as a function of time, as for the VIF curves. The same ROIs for any given rat were used in each analysis.

a) "Pixel-by-pixel ROI" analyses. The intensity values of individual pixels within the ROIs were used in computations. Pixels which demonstrated non-significant changes in signal intensity following contrast agent injection, specifically less than a 50% increase, were not included in further statistical analyses. In addition, positive-definite limits were placed on all fit parameters and any pixels for which fit parameters were outside of such limits were flagged as having fit parameters that were "not a number" (NaN).

b) "Whole ROI" analyses. The average intensity value of the whole tumor ROI was used in computations.

The average of the DCE-MRI parameter values derived from each of the three imaging slices were used in subsequent analyses. Illustrative examples of DCE-MRI parametric maps are presented in Fig 2.

Statistical analyses

Summary statistics of DCE-MRI parameters (K^{trans}, k_{ep}, v_e, and where applicable, v_p) were provided in the form of median and range. All data were transformed to the logarithmic scale, due to right-skewness, prior to statistical analyses.

A linear mixed model was used to assess if each DCE-MRI parameter changed significantly over three days. The linear mixed model took into account the correlation between measurements of the same rat. No statistically significant trend was detected for any DCE-MRI parameter in the span of three days (results not shown).

Comparisons between DCE-MRI parameters by analytical method were also based on linear mixed models. Interactions between analytical methods and time were not significant (results not shown), therefore, analytical methods and time were fit as main effects only. All the

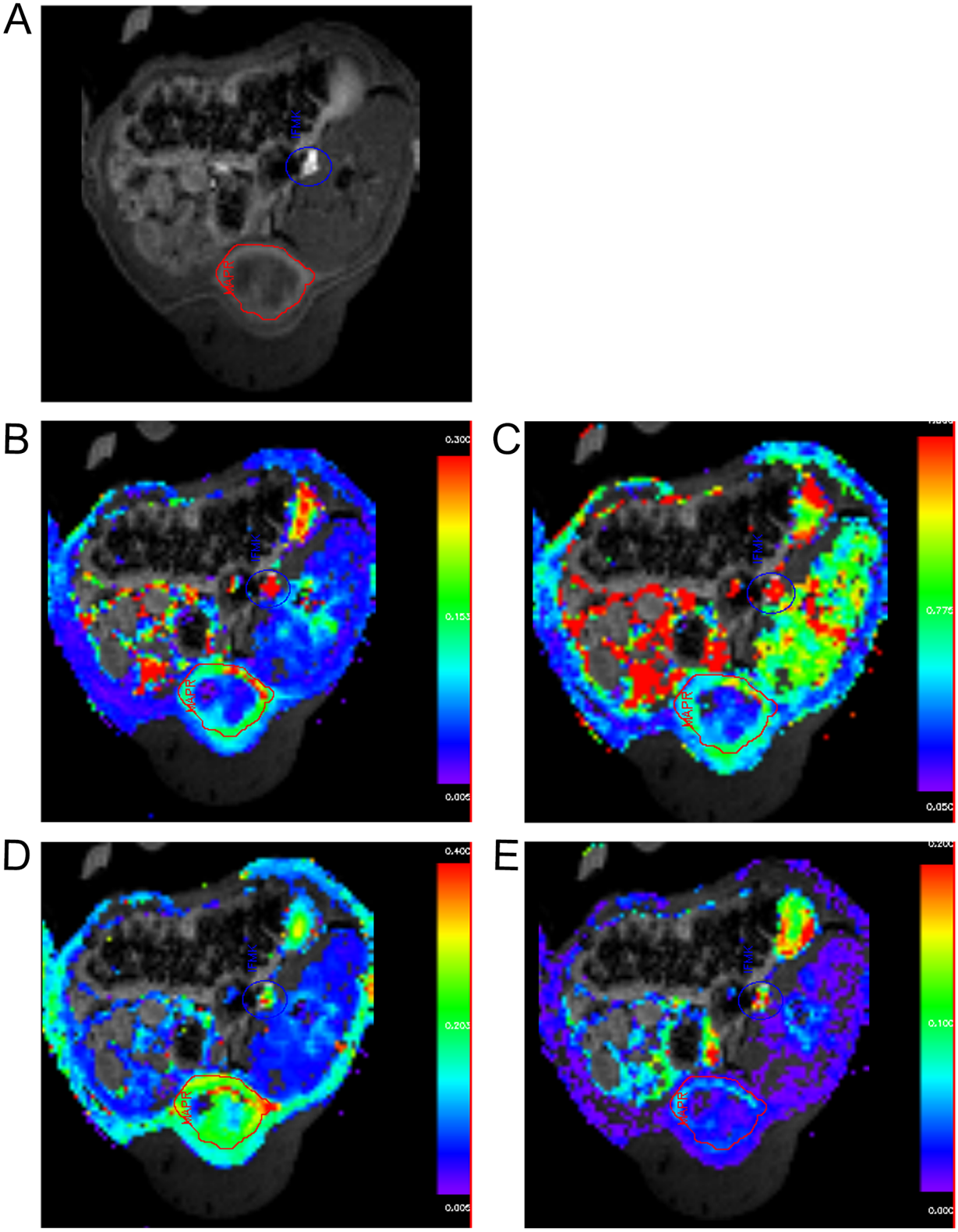

Fig 2. Illustrative parametric maps using 3-parameter physiological model, individual VIF and pixel based analysis. Same animal as Fig 1. A) Source trans-axial DCE-MRI image [blue outline is VIF input mask; red outline is tumor ROI mask]; B) K^{trans}, C) k_{ep}, D) v_e, and E) v_p parameteric maps.

doi:10.1371/journal.pone.0130168.g002

pairwise comparisons between analytical methods were estimated and p-values were adjusted using the Bonferroni method to control the overall type I error rate at 5%.

A variance components analysis was used to estimate the inter- and intra-rat variances. The intra-rat coefficient of variation (wCV) was calculated using the Bland-Altman method [25] as follows: logarithms of the data were taken and within-rat standard deviations estimated, the results were back-transformed to the raw scale (anti-log), and a value of one was subtracted from them to obtain the wCVs.

All statistical analyses were two-sided and *p*-values of 0.05 or less were considered statistically significant. Statistical analysis was carried out using SAS version 9 (SAS Institute, Cary, NC). Plotting was performed using Spotfire S+ 8.2 (TIBCO Software Inc., Somerville, MA).

Results

Summary statistics for the DCE-MRI parameters, by analytic method, are presented in Table 1. Overall, DCE-MRI parameter values varied widely across the various analytical methods, *i.e.* the tracer kinetic model, VIF input, and method of ROI analysis, with the range in median DCE-MRI parameter values as follows: K^{trans}, 0.09–0.18 min^{-1}; k_{ep}, 0.51–0.92 min^{-1}; v_e, 0.17–0.23; and v_p, 0.02–0.04 (Table 1).

The wCV values also varied widely by analytical method, with mean wCVs ranging as follows: K^{trans}, 32.9–61.9%; k_{ep}, 11.6–41.9%; v_e, 16.1–54.9%; and v_p, 53.9–77.2% (Table 1).

Effect of tracer kinetic model: 2-parameter vs. 3-parameter

K^{trans} and k_{ep} were significantly and consistently lower when using the 3-parameter model compared to the 2-parameter model ($p<0.0001$); v_e values were not significantly different (Tables 1 and 2; Fig 3 (green vs. red datasets)).

The effects on repeatability of the DCE-MRI parameters (K^{trans}, k_{ep} and v_e) were comparable, with no significant differences in wCVs across the two tracer kinetic models, as demonstrated by overlapping wCV confidence bounds for corresponding parameters (Table 1).

Effect of VIF: individual- vs. population-based

There were no significant differences in DCE-MRI parameter values (K^{trans}, k_{ep}, v_e, and v_p) when comparing the utilization of individual-based and population-based VIFs in analyses.

Utilization of individual-based VIFs was associated with significantly smaller wCVs for v_e than with the population-based VIF, and conversely for k_{ep} (Fig 3 (1^{st} and 2^{nd} vs. 3^{rd} and 4^{th} columns); Table 1, showing non-overlapping confidence bounds for corresponding wCVs). There were no significant differences for K^{trans} and v_p when comparing individual- vs. population-based VIF analyses.

Effect of ROI: pixel-by-pixel vs. whole tumor

k_{ep} and v_p values were significantly lower for pixel-by-pixel compared to whole ROI analyses ($p<0.0006$), and not significantly different for K^{trans} and v_e values (Tables 1 and 2; Fig 3 (1^{st} and 3^{rd} vs. 2^{nd} and 4^{th} columns)).

There were no significant differences in variability (wCV) between pixel and whole ROI analyses across all the DCE-MRI parameters (K^{trans}, k_{ep}, v_e and v_p).

Between- and within-animal variation

The results of our variance component analyses are presented in Table 3. This shows generally larger intra-rat than inter-rat variances across all DCE-MRI parameters.

Table 1. Summary of DCE-MRI parameter values, by analytical method (n = 12). Model dependent (K^{trans}, k_{ep}, v_e and v_p).

				Whole ROI				Pixel ROI			
VIF	**Parameter model**	**Parameter**	**Units**	**Median**	**IQR**	**Mean wCV %**	**wCV bounds %**	**Median**	**IQR**	**Mean wCV %**	**wCV bounds %**
POP	**2 para**	K^{trans}	min^{-1}	**0.17**	0.10–0.22	**57.8**	38.3–80.0	**0.17**	0.11–0.21	**50.1**	33.5–68.8
		k_{ep}	min^{-1}	**0.92**	0.83–1.03	**14.6***	10.2–18.2	**0.78**	0.73–0.86	**15.8***	11.0–20.9
		v_e	unitless	**0.19**	0.12–0.27	**54.9††**	36.5–75.8	**0.19**	0.14–0.27	**49.0††**	32.8–67.2
POP	**3 para**	K^{trans}	min^{-1}	**0.09**	0.07–0.14	**61.9**	40.9–86.2	**0.10**	0.07–0.14	**53.8**	35.8–74.1
		k_{ep}	min^{-1}	**0.59**	0.54–0.64	**11.6***	8.11–15.2	**0.52**	0.48–0.56	**14.1***	9.8–18.6
		v_e	unitless	**0.17**	0.12–0.26	**53.7††**	35.7–74.0	**0.18**	0.13–0.27	**52.1††**	34.7–71.7
		v_p	unitless	**0.04**	0.03–0.06	**54.5**	36.3–75.3	**0.04**	0.03–0.05	**53.9**	35.9–74.3
INDIV	**2 para**	K^{trans}	min^{-1}	**0.18**	0.15–0.25	**39.7**	26.8–53.8	**0.17**	0.14–0.23	**32.9**	22.4–44.3
		k_{ep}	min^{-1}	**0.85**	0.69–1.07	**33.1****	22.6–44.6	**0.69**	0.58–0.92	**34.3****	23.4–46.3
		v_e	unitless	**0.22**	0.20–0.25	**16.1†**	11.2–21.2	**0.23**	0.20–0.26	**16.9†**	11.7–22.3
INDIV	**3 para**	K^{trans}	min^{-1}	**0.11**	0.09–0.14	**39.3**	26.6–53.3	**0.12**	0.10–0.14	**34.4**	23.4–46.4
		k_{ep}	min^{-1}	**0.56**	0.46–0.69	**36.6****	24.9–49.5	**0.51**	0.39–0.62	**41.9****	28.2–57.0
		v_e	unitless	**0.21**	0.18–0.24	**16.4†**	11.4–21.6	**0.23**	0.20–0.25	**18.7†**	13.0–24.7
		v_p	unitless	**0.03**	0.02–0.06	**58.8**	39.0–81.5	**0.02**	0.01–0.04	**77.2**	50.2–109.02

POP: population averaged VIF

INDIV: individual measured VIF

IQR: inter-quartile range

wCV: within-subject coefficient of variation. Bounds: 95% lower- and upper-confidence limits

n/a: not applicable

* vs ** = significant differences

† vs †† = significant differences

doi:10.1371/journal.pone.0130168.t001

Table 2. Summary of pairwise comparisons between DCE-MRI parameters by analytical method. P-values based on linear mixed model on the logarithmic scale. The linear mixed model took into account correlation between measurements from the same rat. A Bonferroni adjustment was used to control the overall type I error rate, which with 13 pairwise comparisons set the cutoff point for declaring statistical significance as 0.05/13 = 0.0038, which are bolded.

Parameter model	Comparison	Estimate	Standard Error	p-value
K^{trans}	2para *vs*. 3para model	0.449	0.053	**<0.0001**
K^{trans}	Individual *vs*. Population VIF	0.098	0.060	0.129
K^{trans}	Pixel *vs*. Whole ROI	0.002	0.047	0.966
k_{ep}	2para *vs*. 3para model	0.419	0.021	**<0.0001**
k_{ep}	Individual *vs*. Population VIF	-0.064	0.023	0.019
k_{ep}	Pixel *vs*. Whole ROI	-0.145	0.021	**<0.0001**
v_e	2para *vs*. 3para model	0.031	0.031	0.337
v_e	Individual *vs*. Population VIF	0.175	0.051	0.006
v_e	Pixel *vs*. Whole ROI	0.058	0.029	0.066
v_p	Individual *vs*. Population VIF	-0.100	0.108	0.371
v_p	Pixel *vs*. Whole ROI	-0.434	0.091	**0.0006**

doi:10.1371/journal.pone.0130168.t002

Discussion

The parameters evaluated here are widely regarded by drug developers and others as "biomarkers" within the definition introduced by Atkinson et al. [26]. However, to qualify as biomarkers, they must be "objectively quantified" [26]. If different studies derive different values for the same biomarker because of subtle differences in analysis, the "objective quantification" is deficient [27]. This work was undertaken to assess the impact on parameter values and repeatability of commonly utilized analytical methods in the DCE-MRI arena. Specifically, we explored the effects of two commonly utilized tracer kinetic models (2-parameter *vs*. 3-parameter), two VIF options (population- *vs*. individual-based), and two ROI analytical approaches (whole tumor ROI *vs*. pixel-by-pixel tumor ROI). Each, in principle, has its theoretical advantages and disadvantages.

Our results suggest that DCE-MRI parameter values vary widely depending on the analytical methods utilized, in some cases almost two-fold (*e.g*., K^{trans}, k_{ep}, v_p). Overall wCV values also varied widely by analytical methods, with wCVs ranging as follows: K^{trans} 32.9–61.9%; k_{ep}, 11.6–41.9%; v_e, 16.1–54.9%; and v_p, 53.9–77.2%.

In terms of the tracer kinetic models utilized, the 3-parameter model might in principle be expected to provide a more complete reflection of the underlying tracer kinetics compared to the 2-parameter model since it does not neglect the intravascular tracer contribution (*i.e*., the v_p term) as does the 2-parameter model. Our results suggested that the 3-parameter model yielded significantly lower K^{trans} and k_{ep} values than the corresponding 2-parameter model, and no significant differences in v_e values. Since the 2-parameter model neglects the intravascular signal, the bias (i.e. artefactual elevation of K^{trans} and k_{ep} in the 2-parameter model) is not unexpected. Absolute values of K^{trans} and k_{ep} from different studies which use these different models cannot be assumed comparable, even though the same biomarker name and units are reported. There were no significant differences in wCVs for all parameters, which suggests that repeatability was not substantially affected by the physiological model applied for these animals.

With regards to the choice of VIF inputs for the model-based analyses, utilization of individual-based VIFs might be expected to yield more reliable results than using a population-based VIF, since vascular tracer profiles can vary quite widely due to variations in IV contrast delivery, cardiac output, renal function, *etc*. It is quite possible, however, that the theoretical

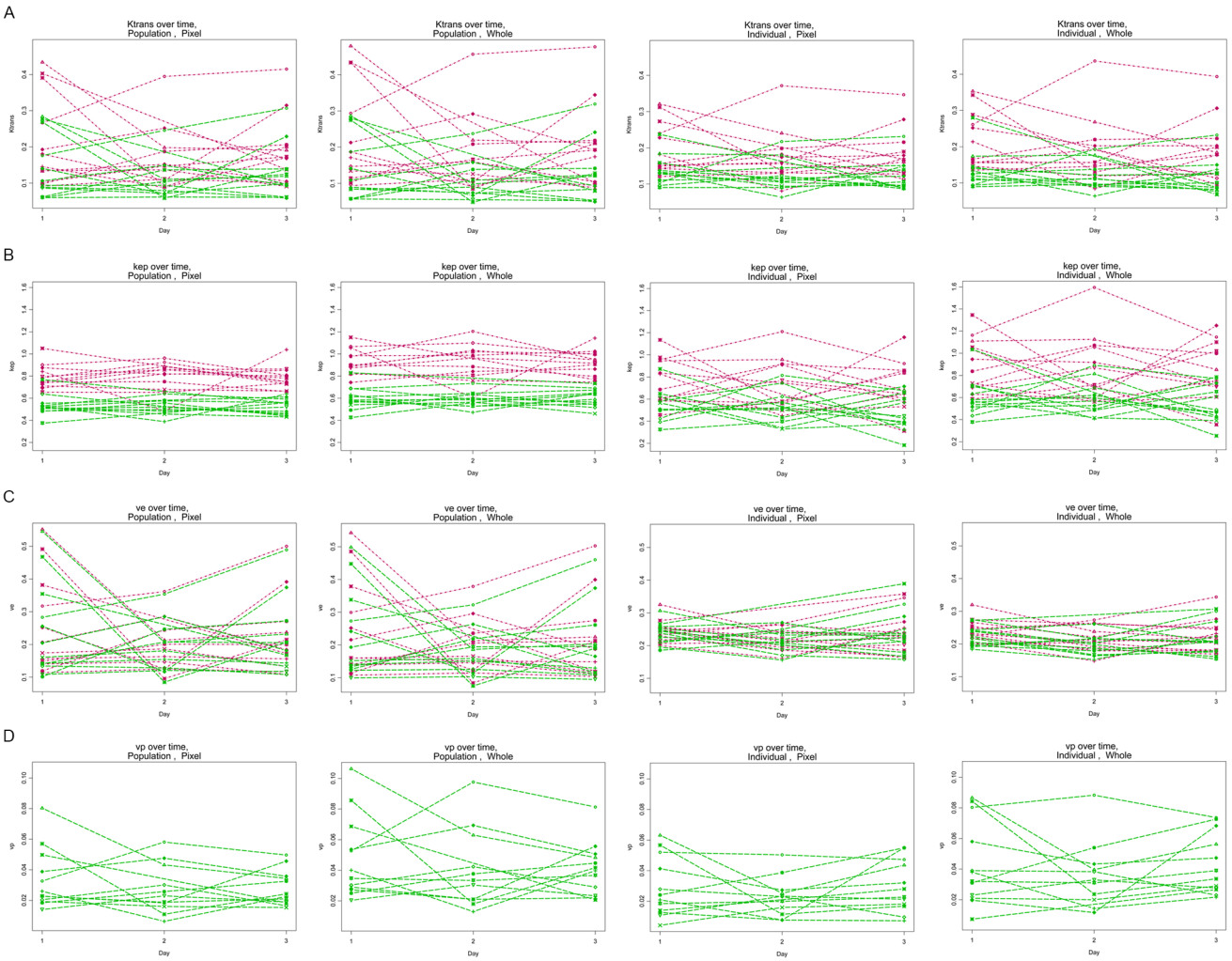

Fig 3. Scatter plots of 3 day time points, of horizontal row a) K^{trans}, b) k_{ep}, c) v_e, d) v_p, by 2- (red lines) vs. 3-parameter (green lines) models; with separate plots for pixel-by-pixel vs. whole tumor analyses, and by individual- vs. population-based VIFs. Y-axes for K^{trans} and k_{ep} in min^{-1}: v_e and v_p, unitless. Note: v_p can only be derived with the 3-parameter model. (Note: one missing data point for one rat)

doi:10.1371/journal.pone.0130168.g003

advantage of utilizing individual-based VIFs might be out-weighed by the substantial technical challenges in obtaining reliable VIFs from DCE-MRI studies. Our results indicated that there were no significant differences in DCE-MRI parameter values obtained between individual- and population-based VIF analyses. However, wCVs when using individual VIFs were significantly smaller for v_e than when using the population VIF, and conversely for k_{ep}. In circumstances in which individually measured VIFs might be unreliable, the utilization of population VIFs may be necessary [19,28]. Our results do not suggest that the use of a population VIF will bias the absolute DCE-MRI biomarker values.

Since each of our DCE-MRI biomarkers is an intensive scalar variable, and since the voxel volumes are identical, the whole-tumor value for each biomarker should in principle be identical to the mean of the individual voxel biomarker values. However, for real-world (noisy) data, that identity may be lost in the propagation of errors, leading to variability and/or bias. Regarding pixel-by-pixel *vs*. whole tumor based ROI evaluations, the former, in principle, is able to display and better reflect the heterogeneous nature of tumors. However, it is computationally

Table 3. Summary of variance components analysis, by analytical method (n = 12). Model dependent (K^{trans}, k_{ep}, v_e and v_p).

			Whole ROI		Pixel ROI	
VIF	**Parameter model**	**Parameter**	**inter-VC**	**intra-VC**	**inter-VC**	**intra-VC**
POP	**2 para**	K^{trans}	0.084	0.208	0.076	0.165
		k_{ep}	0.003	0.018	0.001	0.022
		v_e	0.061	0.191	0.062	0.159
POP	**3 para**	K^{trans}	0.091	0.232	0.083	0.185
		k_{ep}	0.008	0.012	0.004	0.017
		v_e	0.058	0.185	0.058	0.176
		v_p	0.083	0.186	0.081	0.202
INDIV	**2 para**	K^{trans}	0.048	0.112	0.041	0.081
		k_{ep}	0.015	0.082	0.005	0.087
		v_e	0.012	0.022	0.011	0.024
INDIV	**3 para**	K^{trans}	0.000	0.110	0.004	0.088
		k_{ep}	0.000	0.097	0.000	0.122
		v_e	0.010	0.023	0.011	0.029
		v_p	0.142	0.214	0.140	0.327

POP: population averaged VIF

INDIV: individual measured VIF

Inter-VC: between-rat variance component

Intra-VC: within-rat variance component

Intra-VC > inter-VC: indicates that within-rat variation > between-rat variation

n/a: not applicable

doi:10.1371/journal.pone.0130168.t003

more demanding and more vulnerable to signal-to-noise ratio constraints. Furthermore, deriving a simple statistic that adequately summarizes the resultant individual pixel-based parameter distributions is challenging. Adopting the simple approach of using median values to summarize the distributions, our results indicated that pixel-by-pixel based evaluation of ROIs yielded significantly lower k_{ep} and v_p values than whole-tumor based ROI evaluations. As such, it may be important in some circumstances to be able to capture detailed spatial information about tumor heterogeneity.

The tumor time-intensity profile is clearly affected by the tracer input profile. The latter in turn is affected by tracer input delivery (*i.e.*, the intravenous injection) and physiological parameters (*e.g.*, cardiac output and renal/excretion function), all of which can vary between studies. Acquisition of a reliable VIF presents substantial challenges. Difficulties include motion- and flow-related artifacts. The difficulties of acquiring reliable VIFs are compounded in small animal studies by the very small cross-sectional area of the major vessels. Indeed, intensity variations (from noise and artifacts) were evident in our VIF time-intensity plots (Fig 1A). We were able to mitigate the flow related artifacts in our acquisition protocol by application of a saturation band between the site of injection and the imaging volume, but inevitably with some loss of temporal resolution. We took precautions to control for the delivery of intravenous contrast medium. We used a pump injector, with fixed gadolinium and saline flush volumes and flow rates, a fixed site of injection (the tail vein), and a constant length of tubing between the injector and tail vein.

There have been some conflicting reports as to the effect of using individual- compared to population-based VIFs: Rijpkema and co-authors [29] has reported that individual arterial input functions (AIFs), compared to population-based AIFs, improved repeatability of k_{ep}.

Parker and co-authors [28] reported that variation in K^{trans}, v_e, and v_p values were smaller when using a population-based AIF compared to an individual-based AIF in a study of tumors in human patients. Their differing conclusions may be partly due to the relative differences in the consistency of the individual VIFs obtained in their studies. Also a variety of models have been proposed to derive population VIFs, and these two studies employed different approaches. The extent to which such models might influence the conclusions is beyond the scope of this work.

The differing views related to VIF estimations in the studies above in humans are paralleled in the pre-clinical arena. The small blood volume and rapid vascular dynamics inherent to small animals necessitate very rapid sampling schemes in order to accurately capture the peak of intravascular enhancement, corresponding to the maximum concentration of contrast agent after injection, and acquisition strategies that are tuned for rapid AIF sampling generally compromise the spatial resolution and coverage of tumor. Studies utilizing acquisitions that are optimized for AIF measurement with very rapid sampling may provide reduced variability using individual measurements [23,30,31]. In the absence of AIF estimates with high temporal resolution, or in the presence of high noise, repeatability may be improved by use of a parameterized population average [19]. It has also been shown that measurements derived from individual and averaged AIFs correlate strongly when a strictly controlled contrast administration protocol is used [20]. In this work, we employed a 3D acquisition protocol that is biased towards anatomic coverage with relatively slow temporal sampling of the AIF. Our study identified no statistically significant differences in parameter values when using the individual or averaged VIFs, but did find some differences in repeatability (wCV) with some specific parameters.

Previous studies with small animals have reported intra-animal wCVs for K^{trans} and v_e of 18% and 7%, respectively, in a mouse model using PC3 prostate tumors, a 2-parameter model and a pooled (population) VIF [32]. A previous study of ours which compared DCE-MRI and DCE-CT in the same tumor model as in the current study reported wCVs for K^{trans}, k_{ep} and v_e of 23%, 16% and 20% respectively [33]. This study employed a different intravenous injection technique, VIF model and acquisition protocol compared to the current study. The first study above examined repeatability over just two, unlike our three, scan visits in our previous and current studies.

Our variance components analysis allowed us to assess the relative contributions of variations between animals (inter-rat) and between individual scan days (intra-rat), to the overall variation. We found that for all DCE-MRI parameters, the intra-rat contributions were comparable to or larger than the inter-rat contributions to the overall variation in this C6 model. Tumor vasculature is intrinsically chaotic and unstable, and it is not surprising that its day-to-day variations may exceed relatively small between-rat variations, given the uniform and controlled tumor implantation techniques and animals utilized.

We acknowledge and recognize limitations in our study. Our study was undertaken with only one tumor model. The physiological compartment models used in our study are widely used. However, we utilized a single software implementation of these models in this study. It is likely that algorithmic differences within software implementations may give rise to differences in the parameter values.

In our repeatability study, it would have been desirable to obtain scan-rescan measurements in close succession. Unfortunately, any persistent gadolinium would potentially alter signal intensities and saturation, thereby confounding the measurements. It was considered that this difficulty would be mitigated by imposing a one day interval between scans. Unlike other studies which have restricted their evaluations to just two sequential evaluations, we undertook serial imaging evaluations on three consecutive days. Tumors inevitably changed in size and

potentially in their perfusion properties over the 48 hours of our serial imaging. Although we observed increases in tumor size with time, we did not observe any systematic changes in perfusion parameters on formal statistical testing (data not presented). Even if possible, undertaking repeat scans in short succession in one scanner visit would have removed important variables in DCE-MRI experiments, which include handling of animals, anesthesia and physical re-positioning/localization. The variabilities obtained, therefore, more closely mimic longitudinal experiments in which there are typically intervening therapeutic interventions.

We limited our tumor ROI evaluations to a single observer; an examination of inter- and intra-observer variability was beyond the scope of this work. It was also beyond the scope of the current study to explore the impact of our various analytical options with different animal models and DCE-MRI acquisition protocols.

Our results indicate that DCE-MRI parameter values and repeatability can vary widely depending on the specific analytical methods utilized. Comparisons across studies especially of absolute parameter values should be interpreted with caution. Given the wide ranges in variability of parameters, it would be prudent to incorporate scan-rescan repeatability in studies. Efforts should be made to acquire reliable VIF data for analyses. An understanding of repeatability of DCE-MRI measurements provides insight into what observed changes can be considered significant, and can also assist in design of future studies and sample-size calculations.

Acknowledgments

We thank Sandeep N. Gupta, PhD, GE Healthcare, for use of the DCE-MRI analytical software package, Kinmod, under a research agreement, and the staff of the Small Animal Imaging Facility, MD Anderson Cancer Center.

Author Contributions

Conceived and designed the experiments: CSN WW JAB EFJ. Performed the experiments: CSN JAB MKR LH DWB SK. Analyzed the data: CSN WW EFJ. Contributed reagents/materials/analysis tools: JAB MKR LH EFJ. Wrote the paper: CSN WW JAB JCW EFJ.

References

1. O'Connor JP, Jackson A, Parker GJ, Roberts C, Jayson GC (2012) Dynamic contrast enhanced MRI in clinical trials of antivascular therapies. Nat Rev Clin Oncol 9: 167–177. doi: 10.1038/nrclinonc.2012.2 PMID: 22330689
2. Laking GR, West C, Buckley DL, Matthews J, Price PM (2006) Imaging vascular physiology to monitor cancer treatment. Crit Rev Oncol Hematol 58: 95–113. PMID: 16387510
3. O'Connor JP, Jackson A, Parker GJ, Jayson GC (2007) DCE-MRI biomarkers in the clinical evaluation of antiangiogenic and vascular disrupting agents. Br J Cancer 96: 189–195. PMID: 17211479
4. Leach MO, Morgan B, Tofts PS, Buckley DL, Huang W, Horsefield MA, et al. (2012) Imaging vascular function for early stage clinical trials using dynamic contrast-enhanced magnetic resonance imaging. Eur Radiol 22: 1451–1464. doi: 10.1007/s00330-012-2446-x PMID: 22562143
5. Morgan B, Thomas AL, Drevs J, Hennig J, Buchert M, Jivan A, et al. (2003) Dynamic contrast-enhanced magnetic resonance imaging as a biomarker for the pharmacological response of PTK787/ZK 222584, an inhibitor of the vascular endothelial growth factor receptor tyrosine kinases, in patients with advanced colorectal cancer and liver metastases: results from two phase I studies. J Clin Oncol 21: 3955–3964. PMID: 14517187
6. Stevenson JP, Rosen M, Sun W, Gallagher M, Haller DG, Vaughn D, et al. (2003) Phase I trial of the antivascular agent combretastatin A4 phosphate on a 5-day schedule to patients with cancer: magnetic resonance imaging evidence for altered tumor blood flow. J Clin Oncol 21: 4428–4438. PMID: 14645433
7. Evelhoch JL, LoRusso PM, He Z, DelProposto Z, Polin L, Corbett TH, et al. (2004) Magnetic resonance imaging measurements of the response of murine and human tumors to the vascular-targeting agent ZD6126. Clin Cancer Res 10: 3650–3657. PMID: 15173071

8. Willett CG, Boucher Y, di Tomaso E, Duda DG, Munn LL, Tong RT, et al. (2004) Direct evidence that the VEGF-specific antibody bevacizumab has antivascular effects in human rectal cancer. Nat Med 10: 145–147. PMID: 14745444
9. Liu G, Rugo HS, Wilding G, McShane TM, Evelhoch JL, Ng C, et al. (2005) Dynamic contrast-enhanced magnetic resonance imaging as a pharmacodynamic measure of response after acute dosing of AG-013736, an oral angiogenesis inhibitor, in patients with advanced solid tumors: results from a phase I study. J Clin Oncol 23: 5464–5473. PMID: 16027440
10. Tofts PS, Kermode AG (1991) Measurement of the blood-brain barrier permeability and leakage space using dynamic MR imaging. 1. Fundamental concepts. Magn Reson Med 17: 357–367. PMID: 2062210
11. Larsson HB, Stubgaard M, Frederiksen JL, Jensen M, Henriksen O, Paulson OB, et al. (1990) Quantitation of blood-brain barrier defect by magnetic resonance imaging and gadolinium-DTPA in patients with multiple sclerosis and brain tumors. Magn Reson Med 16: 117–131. PMID: 2255233
12. Kety SS (1951) The theory and applications of the exchange of inert gas at the lungs and tissues. Pharmacol Rev 3: 1–41. PMID: 14833874
13. Tofts PS (1997) Modeling tracer kinetics in dynamic Gd-DTPA MR imaging. J Magn Reson Imaging 7: 91–101. PMID: 9039598
14. Weinmann HJ, Laniado M, Mutzel W (1984) Pharmacokinetics of GdDTPA/dimeglumine after intravenous injection into healthy volunteers. Physiol Chem Phys Med NMR 16: 167–172. PMID: 6505043
15. Galbraith SM, Lodge MA, Taylor NJ, Rustin GJ, Bentzen S, Stirling JJ, et al. (2002) Reproducibility of dynamic contrast-enhanced MRI in human muscle and tumours: comparison of quantitative and semi-quantitative analysis. NMR Biomed 15: 132–142. PMID: 11870909
16. Lankester KJ, Taylor NJ, Stirling JJ, Boxall J, D'Arcy JA, Leach MO, et al. (2005) Effects of platinum/taxane based chemotherapy on acute perfusion in human pelvic tumours measured by dynamic MRI. Br J Cancer 93: 979–985. PMID: 16234826
17. Roberts C, Issa B, Stone A, Jackson A, Waterton JC, Parker GJ (2006) Comparative study into the robustness of compartmental modeling and model-free analysis in DCE-MRI studies. J Magn Reson Imaging 23: 554–563. PMID: 16506143
18. Lankester KJ, Taylor JN, Stirling JJ, Boxall J, d'Arcy JA, Collins DJ, et al. (2007) Dynamic MRI for imaging tumor microvasculature: comparison of susceptibility and relaxivity techniques in pelvic tumors. J Magn Reson Imaging 25: 796–805. PMID: 17347990
19. McGrath DM, Bradley DP, Tessier JL, Lacey T, Taylor CJ, Parker GJ (2009) Comparison of model-based arterial input functions for dynamic contrast-enhanced MRI in tumor bearing rats. Magn Reson Med 61: 1173–1184. doi: 10.1002/mrm.21959 PMID: 19253360
20. Loveless ME, Halliday J, Liess C, Xu L, Dortch RD, Whisenant J, et al. (2012) A quantitative comparison of the influence of individual versus population-derived vascular input functions on dynamic contrast enhanced-MRI in small animals. Magn Reson Med 67: 226–236. doi: 10.1002/mrm.22988 PMID: 21688316
21. Ragan DK, Bankson JA. Suppression of vascular enhancement artifacts through the use of a multiband, selectively spoiled radiofrequency excitation pulse. J Magn Reson Imaging 33: 1256–1261, 2011. doi: 10.1002/jmri.22523 PMID: 21509887
22. Ashton EA, Kwok E, Evelhoch J. Conversion from signal intensity to Gd concentration may be unnecessary for perfusion assessment of tumors using DCE-MRI. Proceedings of the 15th Annual Meeting of ISMRM, Berlin, 2007. (abstract 2813)
23. Bradley DP, Tessier JL, Checkley D, Kuribayashi H, Waterton JC, Kendrew J, et al. (2008) Effects of AZD2171 and vandetanib (ZD6474, Zactima) on haemodynamic variables in an SW620 human colon tumour model: an investigation using dynamic contrast-enhanced MRI and the rapid clearance blood pool contrast agent, P792 (gadomelitol). NMR Biomed 21: 42–45. PMID: 17458919
24. Bradley DP, Tessier JJ, Lacey T, Scott M, Jurgensmeier JM, Odedra R, et al. (2009) Examining the acute effects of cediranib (RECENTIN, AZD2171) treatment in tumor models: a dynamic contrast-enhanced MRI study using gadopentate. Magn Reson Imaging 27: 377–384. doi: 10.1016/j.mri.2008.07.021 PMID: 18814988
25. Bland M (2003) Clinical measurement. In: Bland M, editor. An introduction to medical statistics. Oxford: Oxford University Press. pp. 268–275.
26. Atkinson AJ, Colburn WA, DeGruttola VG, DeMets DL, Downing GJ, Hoth DF, et al. (2001) Biomarkers and surrogate endpoints: preferred definitions and conceptual framework. Clin Pharmacol Ther 69: 89–95. PMID: 11240971

27. Waterton JC (2013) Translational Magnetic Resonance Imaging and Spectroscopy: Opportunities and Challenges. In: Garrido L, Beckmann N, editors. New Applications of NMR in Drug Discovery and Development. Cambridge: The Royal Society of Chemistry. pp. 333–360.

28. Parker GJ, Roberts C, Macdonald A, Buonaccorsi GA, Cheung S, Buckley DL, et al. (2006) Experimentally-derived functional form for a population-averaged high-temporal-resolution arterial input function for dynamic contrast-enhanced MRI. Magn Reson Med 56: 993–1000. PMID: 17036301

29. Rijpkema M, Kaanders JH, Joosten FB, van der Kogel AJ, Heerschap A (2001) Method for quantitative mapping of dynamic MRI contrast agent uptake in human tumors. J Magn Reson Imaging 14: 457–463. PMID: 11599071

30. Pickup S, Zhou R, Glickson J (2003) MRI estimation of the arterial input function in mice. Acad Radiol 10: 963–968. PMID: 13678084

31. Ragan DK, Lai SY, Bankson JA (2011) Fast, reproducible measurement of the vascular input function in mice using constrained reconstruction and cardiac sampling. NMR Biomed 24: 373–384. doi: 10.1002/nbm.1601 PMID: 20862661

32. Checkley D, Tessier JJ, Kendrew J, Waterton JC, Wedge SR (2003) Use of dynamic contrast-enhanced MRI to evaluate acute treatment with ZD6474, a VEGF signalling inhibitor, in PC-3 prostate tumours. Br J Cancer 89: 1889–1895. PMID: 14612898

33. Ng CS, Waterton JC, Kundra V, Brammer D, Ravoori M, Han L, et al. (2012) Reproducibility and comparison of DCE-MRI and DCE-CT perfusion parameters in a rat tumor model. Technol Cancer Res Treat 11: 219–288.